https://doi.org/10.5194/egusphere-2025-32
Preprint. Discussion started: 21 March 2025

The Biogeophysical Effects of Carbon Fertilization of the Terrestrial Biosphere

Robert J. Allen[1*]

[1]Department of Earth and Planetary Sciences, University of California, Riverside USA

[*]*Correspondence to*: R. J. Allen (rjallen@ucr.edu)

Abstract

The response of the terrestrial biosphere to increasing atmospheric carbon dioxide (CO_2), i.e., the carbon fertilization effect represents a significant source of uncertainty in future climate projections. The climate impacts of carbon fertilization include cooling associated with the biogeochemical effects of enhanced land carbon storage, whereas the non-carbon cycle biogeophysical effects associated with changes in surface energy and turbulent heat fluxes may warm or cool the climate system. Here, I analyze 15 state-of-the-art Earth system models that conducted simulations driven by 1% per year increases in atmospheric CO_2 concentration that isolate the CO_2 fertilization effect (i.e., CO_2 radiative effects are not active). At the time of CO_2 quadrupling, the biogeophysical effects yield multimodel global mean near-surface warming of 0.16 ± 0.09 K with 13 of the 15 models yielding warming. Most of this warming is associated with decreases in surface latent heat flux associated with reduced canopy transpiration. Decreases in surface albedo and increases in downwelling shortwave and longwave radiation—both of which are modulated by cloud reductions—are also associated with the warming. Overall, however, the biogeophysical warming is about an order of magnitude smaller than the corresponding cooling associated with enhanced land carbon storage at -1.38 K (-1.92 to -0.84 K).

Short Summary

CMIP6 models are analyzed to quantify the biogeophysical (non-carbon cycle) and biogeochemical (enhanced carbon storage) effects of carbon fertilization at the time of CO_2 quadrupling. The biogeophysical effects lead to relatively weak warming (0.16 ± 0.09 K) largely due to decreases in surface latent heat flux associated with reduced canopy transpiration. Biogeochemical cooling associated with enhanced land carbon storage dominates at -1.38 K (-1.92 to -0.84 K).

https://doi.org/10.5194/egusphere-2025-32
Preprint. Discussion started: 21 March 2025

1. Introduction

Over land, increasing atmospheric CO_2 concentrations are associated the carbon fertilization effect (e.g., Ainsworth and Long, 2005; Ainsworth and Rogers, 2007; Leakey et al. 2009; Norby and Zak, 2011). This effect involves physiological and structural vegetation changes including reduced stomatal conductance and increased photosynthesis rates which are expected to increase net primary productivity (NPP) and carbon storage. However, the carbon fertilization effect depends on many factors, including plant species, temperature, and availability of water and nutrients. The availability of soil inorganic nitrogen (N), for example, exerts a strong control on plant productivity and carbon storage in many temperate and boreal ecosystems (Vitousek and Howarth, 1991; Oren et al., 2001; Fernández-Martínez et al., 2014; Kicklighter et al., 2019). Nonetheless, intensification of terrestrial biospheric activity, including increased global photosynthesis and "greening" of the planet, has been found in several recent studies (Forkel et al., 2016; Thomas et al., 2016; Zhu et al., 2016, Campbell et al., 2017; Keeling et al., 2017; Haverd et al., 2020; Walker et al., 2021; Chen et al., 2022; Keenan et al., 2023).

Enhanced land carbon storage and greening of the terrestrial biosphere under elevated atmospheric CO_2 concentrations will promote a biogeochemical cooling effect. In other words, the carbon-concentration feedback, which quantifies the carbon cycle's response to changes in atmospheric CO_2 concentration (expressed in units of carbon uptake/release per unit change in atmospheric CO_2 concentration) is negative from the atmosphere's perspective (Arora et al., 2020). Such changes in the terrestrial biosphere will also drive biogeophysical effects associated with surface energy and turbulent heat fluxes. For example, structural vegetation changes (e.g., enhanced leaf area index, LAI) associated with carbon fertilization will impact surface physical properties. This includes altered surface albedo, e.g., plants are darker than bare soil (Betts et al., 2000, Bala et al., 2006; Li et al., 2015), which promotes enhanced surface absorption of solar radiation and hence warming. Furthermore, the physiological changes of carbon fertilization (i.e., reduced stomatal conductance and enhanced water use efficiency) are associated which reduced plant transpiration and latent heat flux, which directly impact surface temperature (i.e., less evapotranspiration implies surface warming) as well as atmospheric water vapor and clouds (Field et al., 1995; Bounoua et al., 1999; Cao et al., 2010; Doutriaux-Boucher et al., 2009). Thus, the overall impact of carbon fertilization on surface temperature is determined by a combination of biogeochemical (carbon cycle) effects and biogeophyscial (non-carbon cycle) effects.

In this paper, I use 15 Coupled Model Intercomparison Project phase 6 (CMIP6; Eyring et al., 2016) models to quantify the climate effects of carbon fertilization, i.e., in the absence of the direct radiative effects of CO_2. Climate effects include the directly simulated biogeophysical (non-carbon cycle) temperature response as well as the drivers, while I infer the biogeochemical temperature response. I find significant global mean biogeophysical warming, largely driven by reductions in latent heat flux associated with decreases in canopy transpiration. Decreases in surface albedo and increases in downwelling shortwave and longwave radiation (which are modulated by cloud reductions) are also associated with the warming. The magnitude of this biogeophysical warming, however, is about an order of magnitude smaller than the inferred biogeochemical cooling associated with enhanced land carbon storage.

https://doi.org/10.5194/egusphere-2025-32
Preprint. Discussion started: 21 March 2025

2. Methods

2.1 CMIP6 Models and 1% per Year Simulations

CMIP6 (Eyring et al., 2016) performed three sets of 1% per year increasing atmospheric CO_2 concentration simulations (1PCTCO$_2$), which are initialized from the preindustrial CO_2 concentration of ~284 ppm and integrated for 150 years. The default 1PCTCO$_2$ simulations are fully coupled as the radiation and carbon cycle components see the increasing CO_2 concentration. Two variants of the 1PCTCO$_2$ simulation were performed as part of the Coupled Climate-Carbon Cycle Model Intercomparison Project (C4MIP; Jones et al., 2016), including a biogeochemically coupled version (1PCTCO$_2$-bgc) and a radiatively coupled version (1PCTCO$_2$-rad). Under 1PCTCO$_2$-bgc, only the carbon cycle components (both land and ocean) respond to the increase in CO_2, while the atmospheric radiative transfer calculations use a CO_2 concentration that remains at the preindustrial concentration. Under 1PCTCO$_2$-rad, only the atmospheric radiation code sees the increase in CO_2 and the carbon cycle components see the fixed, pre-industrial CO_2 concentration.

The focus of this analysis is on the 1PCTCO$_2$-bgc runs, which allows assessment of the climate responses associated with the carbon cycle under elevated CO_2 (without the influence of CO_2 radiative effects). Over land, this effect is traditionally referred to as carbon fertilization of the terrestrial biosphere (e.g., Ainsworth and Long, 2005; Ainsworth and Rogers, 2007; Forkel et al., 2016; Thomas et al., 2016; Zhu et al., 2016, Campbell et al., 2017; Chen et al., 2022). In particular, this includes changes in vegetation physiology including photosynthesis, transpiration and stomatal conductance, and changes in vegetation state (e.g., leaf area index, canopy height). In models with dynamic vegetation, this also includes changes in vegetation type and coverage. These changes in turn affect surface radiative and turbulent heat fluxes which impact surface temperature and other aspects of climate. As the three sets of 1PCTCO$_2$ simulations are CO_2 concentration driven (as opposed to emissions driven), the simulated climate responses include only the biogeophysical effects (e.g., changes in surface fluxes and more generally all non-carbon cycle effects). The climate impacts associated with changes in terrestrial carbon pools (biogeochemical effects) are not allowed to feedback onto the climate system (i.e., enhanced land carbon storage under elevated CO_2 does not impact the atmospheric CO_2 concentration and thus does not impact climate). However, as discussed below, the surface temperature responses to changes in terrestrial carbon pools can be inferred from the transient climate response to cumulative CO_2 emissions (TCRE; Gillett et al., 2013; Arora et al., 2020; Boysen et al. 2020).

This analysis uses 15 CMIP6 models (Supplementary Table 1). Responses are estimated from years 101-140 (CO_2 quadruples in year 140) in the 1PCTCO$_2$-bgc runs relative to the corresponding 40 years in the preindustrial control simulation. I refer to this 40-year time period as the time of CO_2 quadrupling. Preindustrial control simulations feature fixed (to the preindustrial value) atmospheric CO_2 concentration and other climate drivers (e.g., other greenhouse gases, solar irradiance, aerosols). Monthly mean data is used and all data is interpolated to a 2.5°x2.5° grid and aggregated to annual means. Only two models, GFDL-ESM4 and MPI-ESM1-2-LR, include dynamic vegetation (i.e., vegetation type and coverage can respond to the elevated CO_2). Three models, GFDL-ESM4, UKESM1-0-LL and NorESM2-LM, include atmospheric chemistry with an interactive representation vegetation biogenic volatile organic compound (BVOC) feedbacks (e.g., Gomez et al., 2023). Eight models, including

https://doi.org/10.5194/egusphere-2025-32
Preprint. Discussion started: 21 March 2025

ACCESS-ESM1-5, CESM2, CMCC-ESM2, EC-Earth3-CC, MIROC-ES2L, MPI-ESM1-2-LR, NorESM2-LM and UKESM1-0-LL, feature a terrestrial nitrogen cycle (Supplementary Table 1). Additional model information can be found in Arora et al. (2020); Gomez et al. (2023); Allen et al. (2024) and Gier et al. (2024).

2.2 Surface Energy Balance Decomposition

The Surface Energy Balance (SEB) decomposition (Luyssaert et al., 2014; Hirsch et al., 2018; Boysen et al., 2020) is used to infer the contribution of changes in energy fluxes to changes in surface temperature (ΔTS):

$$\Delta TS = \frac{1}{4\epsilon\sigma TS_{control}^3}[\Delta SWD(1-\alpha) - \Delta\alpha(SWD) + \Delta LWD - \Delta LH - \Delta SH],$$

where ε is the surface emissivity assumed to be 0.97 (Boysen et al., 2020), σ is the Stefan-Boltzmann constant with a value of 5.67×10^{-8} W m^{-2} K^{-4}, and $TS_{control}$ is the surface temperature from the preindustrial control experiment. The first term in square brackets represents the contribution from changes in downwelling surface shortwave radiation (ΔSWD) which is multiplied by the monthly mean climatology of (1-α); the second term represents the contribution from changes in surface albedo (α) which is multiplied by the monthly mean SWD climatology (changes in albedo impact upwelling surface shortwave radiation); the third term represent the contribution from changes in downwelling surface longwave radiation (ΔLWD); the fourth term represents the contribution from changes in surface latent heat flux (ΔLH); and the final term represents the contribution from changes in surface sensible heat flux (ΔSH). I also decompose the first term on the right (i.e., the surface downwelling SW radiation term) into the contribution from changes in surface downwelling shortwave radiation under clear-sky and cloudy-sky conditions. The clear-sky contribution is estimated as $\Delta SWD_{clear}(1-\alpha)$, where ΔSWD_{clear} is the change in clear-sky downwelling surface solar radiation. The cloudy-sky contribution is estimated as the residual between the all-sky and clear-sky SWD radiation SEB components. A similar decomposition is performed for downwelling surface longwave radiation to isolate its clear-sky and cloudy-sky contributions. The SEB decomposition is performed over all land areas. I note that the SEB decomposition does not account for all factors, including for example the ground heat flux and changes in subsurface heat storage (both of which are assumed to be zero here), or changes in surface emissivity.

2.3 Statistical Significance

Statistical significance of a response is estimated using two approaches. In the first approach (e.g., Fig. 1), the multimodel mean time series for the experiment and the control is calculated and their difference is computed. A 2-tailed pooled t-test is used to assess significance of this difference at the 90% confidence level with n_1+n_2-2 degrees of freedom (n_1 is the number of years in the experiment and n_2 is the number of years in the control, i.e., 40 years each) using the pooled variance $\frac{(n_1-1)S_1^2+(n_2-1)S_2^2}{n_1+n_2-2}$, where S_1 and S_2 are the sample variances. Significance of the multimodel mean response relative to each individual model response (e.g., Supplementary Table 2) is estimated by comparing the average of the individual model responses relative to its uncertainty, estimated as $\pm 1.65 \times SE$ (i.e., the 90% confidence interval). SE is the standard

https://doi.org/10.5194/egusphere-2025-32
Preprint. Discussion started: 21 March 2025

error estimated as $\frac{1.65\times\sigma}{\sqrt{m}}$, where σ is the standard deviation across models and *m* is the number of models. Model agreement on the sign of the multimodel mean response is spatially and globally estimated as the percentage of models that yield a positive or negative response. A 2-tailed binomial test yields model agreement at the 90% confidence level when at least 11 of the 15 (73%) models agree on the sign of the response. Significance of correlations (*r*) is estimated from a two-tailed t-test as: $t = \frac{r}{\sqrt{\frac{1-r^2}{N-2}}}$, with *N-2* degrees of freedom. N is either the number of grid boxes (for a spatial correlation) or the number of models (for correlations across models).

3. **Results**

3.1 Vegetation, Land Carbon and Inferred Biogeochemical Temperature Responses

Figure 1 shows multimodel mean annual mean responses of vegetation including NPP and LAI. The global mean increase in NPP is 679.4 ± 140.6 kg km^{-2} day^{-1} (77.4% increase relative to the control) with larger increases in the tropics (30S-30N) at 1049.7 ± 248.2 kg km^{-2} day^{-1} as compared to the extratropics (30S-60S and 30N-60N) at 516.7 ± 109.4 kg km^{-2} day^{-1} (Supplementary Table 2). In each of these regions, all 15 models agree on a positive NPP response (Supplementary Figure 1 shows the spatial model agreement on the sign of the response). Similar results exist for LAI with a multimodel mean global mean increase of 0.71 ± 0.25 (Fig. 1b; 48.9% increase relative to the control), which increases to 1.12 ± 0.41 in the tropics. Here, however, one model features a decrease in LAI (GISS-E2-1-G). One of the two models with interactive vegetation, GFDL-ESM4, yields relatively large global mean NPP increases (2nd largest) at 1207.3 ± 30.9 kg km^{-2} day^{-1} (global mean) whereas MPI-ESM1-2-LR yields 673.2 ± 13.9 kg km^{-2} day^{-1}, a value close to the multimodel global mean increase. In terms of LAI, GFDL-ESM4 yields a value close to the multimodel global mean at 0.84 ± 0.02 while MPI-ESM1-2-LR yields the weakest global mean increase at 0.17 ± 0.01. Thus, there are not clear model differences in these vegetation responses between those models with interactive vegetation versus those models that lack interactive vegetation.

In terms of land carbon (cLand), the multimodel annual mean global mean increase is 4.52 ± 0.68 kgC km^{-2} and all 14 models (GISS-E2-1-G is missing) agree on enhanced land carbon sequestration. Decomposing land carbon into vegetation, soil organic matter and litter carbon shows that the bulk of this increase is due to an increase in vegetation carbon (Fig. 1e) at 2.48 ± 0.42 kgC km^{-2} (75.1% increase relative to the control). This is followed by an increase in soil organic matter carbon (Fig. 1d) at 1.38 ± 0.49 kgC km^{-2} (15.0% increase relative to the control) and litter carbon (Fig. 1c) at 0.66 ± 0.22 kgC km^{-2} (64.4% increase relative to the control). Converting the above land carbon responses into multimodel mean global totals yields 468.1 ± 89.4 PgC; 248.0 ± 89.5 PgC; and 119.1 ± 45.2 PgC for vegetation carbon, soil carbon and litter carbon, respectively. Thus, the total land carbon increase is 835.3 ± 134.3 PgC. Increases in vegetation carbon contribute 56% to this value, followed by soil carbon at 30% and litter carbon at 14%. Once again, models with interactive vegetation do not stand out, as GFDL-ESM4 yields a total land carbon increase of 958.6 ± 32.6 PgC and MPI-ESM1-2-LR yields 530.7 ± 12.0 PgC (4th smallest increase).

https://doi.org/10.5194/egusphere-2025-32
Preprint. Discussion started: 21 March 2025

I separate the models into the eight (N models) that have a representation of the terrestrial nitrogen cycle versus the six models (noN models) that do not (GISS-E2-1-G is missing so there are only 14 models). As noted in Gier et al. (2024), the inclusion of nitrogen limitation led to a large improvement in photosynthesis compared to models not including this process.
I find significantly larger increases in land carbon storage in noN models at 1153.4 ± 213.6 PgC versus 581.6 ± 157.5 PgC in N models (consistent with Arora et al., 2020). Similar but less significant statements apply for NPP (923.4 ± 202.2 kg km^{-2} day^{-1} in noN models versus 679.4 ± 140.6 kg km^{-2} day^{-1} in N models) and LAI (0.94 ± 0.48 in noN models versus 0.62 ± 0.24 in N models). The weaker increase in land carbon storage in models with a terrestrial nitrogen cycle is consistent with terrestrial nitrogen generally reducing the response of NPP and carbon storage to elevated levels of atmospheric CO_2 because of an increasing limit of nitrogen availability for carboxylation enzymes and new tissue construction (e.g., Jones et al., 2016).

I use the TCRE (Gillett et al., 2013; Arora et al., 2020; Boysen et al. 2020) to estimate the near-surface air temperature (TAS) response to the aforementioned changes in land carbon (biogeochemical effects). The TCRE quantifies the amount of warming relative to the preindustrial state per unit cumulative emissions at the time when atmospheric CO_2 concentration doubles in the 1PCTCO$_2$ simulation. The best estimate of the TCRE at 1.65 K per 1000 PgC, with a likely range from 1.0 to 2.3 K per 1000 PgC (Canadell et al., 2021) yields a biogeochemical cooling effect of -1.38 (-1.92 to -0.84) K. Models without a terrestrial nitrogen cycle (consistent with their enhanced land carbon storage) yield larger cooling (but not significantly so) at -1.90 (-2.65 to -1.15) K relative to the models with a terrestrial nitrogen cycle at -0.96 (-1.34 to -0.58) K. Similar biogeochemical cooling is obtained if I use an estimate of each model's TCRE (as opposed to the best estimate) at -1.22 K for all models; -1.70 K for noN models; and -0.86 K for N models. Thus, the cooling difference between models with and without a terrestrial nitrogen cycle is largely due to differences in the land carbon response.

Thus, carbon fertilization at the time of CO_2 quadrupling yields large increases in land carbon storage and corresponding global mean biogeochemical cooling as inferred from the TCRE. Models that lack a terrestrial nitrogen cycle tend to yield larger increases in land carbon storage and in turn, larger inferred cooling, implying they may overestimate the magnitude of this cooling effect. I note that the magnitude of this multimodel biogeochemical mean cooling is relatively large, e.g., it is about 35% of the global mean warming under 1PCTCO$_2$ and 1PCTCO$_2$-rad (which only accounts for the radiative effect of CO_2) of 3.94 ± 0.37 K and 3.78 ± 0.35 K, respectively.

3.2 Biogeophysical Temperature Responses

Figure 2a shows the multimodel annual mean near-surface air temperature response. As noted above, the simulated temperature responses in these simulations includes only the biogeophysical (non-carbon cycle) effects. The multimodel annual mean global mean TAS response is 0.16 ± 0.09 K with 13 of the 15 models yielding warming (Fig. 2b shows the spatial model agreement on the sign of the response). The largest warming occurs in EC-Earth3-CC at 0.51 ± 0.05 K, followed by CESM2 at 0.44 ± 0.04 K and UKESM1-0-LL at 0.40 ± 0.04 K (Supplementary Figure 2). The two models that yield cooling are CMCC-ESM2 and CNRM-ESM2-1 at -0.01 ± 0.07 (not significant at the 90% confidence level) and -0.31 ± 0.04 K, respectively

https://doi.org/10.5194/egusphere-2025-32
Preprint. Discussion started: 21 March 2025

(Supplementary Figure 2e,f). Over land, the multimodel mean warming increases to 0.28 ± 0.13 K (14 of the 15 models yield warming). In both cases, warming is larger in the extratropics as compared to the tropics (Supplementary Table 3). Thus, biogeophysical effects of carbon fertilization yield warming, but much less as compared to the corresponding biogeochemical effects noted above at -1.38 (-1.92 to -0.84) K. I also note that the biogeophysical warming of carbon fertilization is much smaller as compared to the biogeophysical warming associated with the radiative effects (from 1PCTCO$_2$-rad simulations) of CO_2 at 3.78 ± 0.35 K.

3.3 Drivers of the Biogeophysical Temperature Response

I use the surface energy balance (SEB; Section 2.2) decomposition (Luyssaert et al., 2014; Hirsch et al., 2018; Boysen et al., 2020) to understand the drivers of the biogeophysical temperature changes. I first note that the SEB decomposition reasonably reproduces the change in surface temperature (TS) and TAS. For example, the SEB reconstructed multimodel annual mean global land mean TS response is 0.33 ± 0.13 K relative to the actual TS and TAS responses of 0.26 ± 0.12 K and 0.28 ± 0.13 K, respectively (Supplementary Table 4).

Figure 3 shows multimodel annual mean spatial responses for the main terms of the SEB decomposition (Supplementary Figure 3 shows the corresponding model agreement on the sign of the responses). The surface latent heat flux (LH) term (Fig. 3d) at 0.27 ± 0.11 K (Supplementary Table 4) contributes the most to the global land warming, followed by the downwelling surface longwave radiation (LW) term (Fig. 3c) at 0.20 ± 0.13 K. The surface albedo (α) term (Fig. 3a) contributes 0.11 ± 0.06 K and the downwelling surface shortwave radiation (SW) term (Fig. 3b) contributes 0.09 ± 0.06 K. In contrast, the surface sensible heat flux (SH) term (Fig. 3e) leads to cooling at -0.34 ± 0.08 K. Model agreement on the sign of the multimodel mean response occurs in 12 to 13 of the 15 models (depending on the SEB term; Supplementary Table 4). As with the global land mean, the LH SEB term at 0.45 ± 0.15 K contributes the most to the tropical land mean warming (14/15 models agree on warming). Over extratropical land, the dominant SEB terms are the LW term (0.20 ± 0.16 K), as well as the surface albedo (0.16 ± 0.09 K) and SW terms (0.16 ± 0.10 K).

The large warming due to the LH SEB term, which can be decomposed into canopy transpiration and evaporation (which includes sublimation) SEB terms, is consistent with decreased canopy transpiration due to decreased stomatal conductance under the higher atmospheric CO_2 concentration, i.e., more efficient stomata that lose less water to the atmosphere (e.g., Wong et al., 1979; Keenan et al., 2013). Figure 4 shows additional terms from the SEB decomposition, including relatively large values for the transpiration SEB term (Fig. 4e; corresponding model agreement spatial maps are included in Supplementary Figure 4). The multimodel global land mean increase in the canopy transpiration SEB term is 0.45 ± 0.15 K (13 of the 13 models agree on the increase; Supplementary Table 4), which increases to 0.70 ± 0.26 K in the tropics. Warming associated with decreased canopy transpiration is muted to some extent through increases in evaporation (which cools). The corresponding evaporation SEB term over global land yields cooling of -0.19 ± 0.16 K, but with reduced model agreement on the cooling (9 of 13 models). This again increases in magnitude over tropical land to -0.26 ± 0.25 K but with only 7 of 13 models agreeing on the cooling. The enhanced evaporation appears to be directly related to the decrease in transpiration. Spatially correlating the multimodel mean change in the transpiration and evaporation SEB terms yields a very strong global land correlation of -0.83,

https://doi.org/10.5194/egusphere-2025-32
Preprint. Discussion started: 21 March 2025

which increases to −0.86 over tropical land. Similar results exist across models, i.e., the correlation between each model's transpiration and evaporation SEB terms is −0.69 over global land, which increases to −0.78 over tropical land (correlations are significant at the 99% confidence level). This suggests that for conditions of reduced transpiration, evaporation increases to try to satisfy the evaporative demand of the atmosphere.

Although all of the SEB terms may contain temperature induced feedbacks to some extent (since these are coupled ocean-atmosphere simulations), warming associated with the LW SEB term (particularly its clear-sky component) is likely a response to the surface warming as opposed to a driver of the warming. Surface warming will lead to an increase in upwelling LW radiation consistent with the Stefan-Boltzmann law whereby a blackbody radiates energy proportional to TS^4. Some of this enhanced upwards longwave radiation (via the atmospheric greenhouse effect) will be reradiated back down to the surface, i.e., enhanced downwelling LW radiation at the surface. This argument is consistent with Vargas Zeppetello et al. (2019), who found surface downwelling LW radiation is tightly coupled to surface temperature. Changes in the LW SEB term are also likely augmented by increases in atmospheric water vapor via the water vapor feedback (i.e., a stronger greenhouse effect). For example, the multimodel global mean tropospheric specific humidity significantly increases by 0.017 ± 0.014 g kg^{-1} (increases also occur over land but these are not significant; Supplementary Table 3; Supplementary Figure 5f).

I also note that the cooling under the SH SEB term is likely in part a feedback to the surface warming as well as a response to the warming under the LH SEB term. In the former case, surface warming (largely induced by decreases in surface latent heat flux, decreases in surface albedo and increases in solar radiation) will lead to an increase in sensible heat flux, which will act to cool the surface. In the latter case, a reduction in latent heat flux will be compensated by an increase in sensible heat flux. Spatially correlating the multimodel mean change in the SH and LH SEB terms yields a very strong global land correlation of −0.90, which increases to −0.92 over tropical land. Similar results exist across models, i.e., the correlation between each model's SH and LH SEB terms is −0.84 over global land, which increases to −0.86 over tropical land (correlations are significant at the 99% confidence level). Thus, these correlations support an inverse relationship between the SH and LH SEB responses. As the LH SEB term leads to warming consistent with reduced stomatal conductance under elevated CO_2, this is in part compensated for by SH SEB cooling.

The LW SEB term can be decomposed into clear-sky (LW_{clear}; Fig. 4c) and cloudy-sky (LW_{cloud}; Fig. 4d) contributions. All of the multimodel mean global land warming associated with the LW SEB term is due to the LW_{clear} SEB component at 0.27 ± 0.13 K (12 of 14 models agree on the warming). The dominance of the LW_{clear} SEB term warming is consistent with the aforementioned greenhouse effect, combined with increased atmospheric water vapor. In contrast, the LW_{cloud} SEB term contributes to multimodel mean global land cooling of -0.07 ± 0.03 K (12 of 14 models agree on the cooling). This cooling is consistent with a multimodel mean global land decrease in total cloud cover at -0.52 ± 0.23 % (12 of 15 models agree on the decrease; Supplementary Figure 5a and 6a). A decrease in cloud cover will act similarly to the greenhouse effect (i.e., here a weaker greenhouse effect) and this will promote a decrease in surface downwelling LW radiation. Consistently, larger multimodel mean LW_{cloud} SEB cooling

https://doi.org/10.5194/egusphere-2025-32
Preprint. Discussion started: 21 March 2025

occurs in the extratropics at -0.11 ± 0.05 K, consist with the larger decrease in extratropical total cloud cover at -0.64 ± 0.29 %.

I note that the multimodel mean decrease in global land cloud cover is consistent with the previously discussed decrease in latent heat flux (largely due to decreases in canopy transpiration) and with decreases in near-surface and tropospheric relative humidity over land (Supplementary Figure 5c,d and 6c,d). For example, the multimodel mean global land decrease in near-surface relative humidity is -0.87 ± 0.48 %, which increases in magnitude (as does canopy transpiration) to -1.09 ± 0.59 % over tropical land (11 of 14 models agree on both decreases). The corresponding decrease in multimodel mean global land tropospheric relative humidity is weaker but still significant at -0.21 ± 0.12 % (12 of 14 models agree on the decrease). The near-surface relative humidity decrease over land is consistent with near-surface land warming (which increases the water vapor carrying capacity of the air) and with a (non-significant) decrease in near-surface specific humidity (-0.010 ± 0.052 g kg^{-1}; Supplementary Figure 5e and 6e). The tropospheric relative humidity decrease over land is consistent with tropospheric warming (0.18 ± 0.09 K) dominating over non-significant increases in tropospheric specific humidity (0.011 ± 0.015 g kg^{-1}; Supplementary Figure 5f and 6f). In other words, the thermodynamic increase in water vapor over land as dictated by the Clausius Clapeyron equation (e.g., water vapor increases by 7% per K of warming) is muted by the decrease in latent heat flux, and in particular canopy transpiration. I also note a multimodel mean decrease in global land precipitation (Supplementary Figure 5b and 6b) at -0.028 ± 0.017 mm day^{-1} (-1.2 % change relative to the control) with 12 of 15 models agreeing on the decrease.

Warming associated with the surface albedo SEB term is consistent with surface darkening (e.g., Betts et al., 2000, Bala et al., 2006; Li et al., 2015) under enhanced vegetation (e.g., LAI increases; Fig. 1b). In contrast to maximum tropical warming due to the LH SEB term, warming associated with the surface albedo SEB term is largest in the extratropics. The corresponding multimodel mean extratropical land warming is 0.16 ± 0.09 K relative to the tropical warming of 0.06 ± 0.04 K. Larger extratropical as opposed to tropical warming under the surface albedo SEB term is consistent with larger vegetation-induced darkening over higher latitudes, where snow and ice (bright surfaces with high surface albedo) are more prevalent.

The SW SEB term, which yields multimodel mean global land warming of 0.09 ± 0.06 K (12 of 15 models agree on the warming), can be decomposed into clear-sky (SW_{clear}; Fig. 4a) and cloudy-sky (SW_{cloud}; Fig. 4b) contributions. In contrast to the total SW SEB term, the SW_{clear} SEB term yields multimodel mean global land cooling at -0.05 ± 0.02 K. Such cooling is consistent with the aforementioned increase in tropospheric specific humidity, which increases the atmospheric absorption of shortwave radiation by water vapor. Changes in atmospheric aerosols may also contribute though direct scattering/absorption of solar radiation. Few models, however, archived the relevant aerosol diagnostics and changes in the multimodel mean aerosol optical depth (AOD; Supplementary Figure 7) lack significance except for tropical land (Supplementary Table 3). For example, a nonsignificant multimodel global land AOD increase of 1.88 ± 2.50 10^{-3} occurs, with 5 of the 8 models agreeing on the increase. This increases and becomes significant over tropical land at 3.07 ± 3.00 10^{-3} (5 of 8 models agree on the increase). Part of these AOD increases are due to (nonsignificant) increases in dust AOD (DAOD; Supplementary Table 3). If I remove DAOD from (total) AOD (i.e., $AODNOD = AOD -$

https://doi.org/10.5194/egusphere-2025-32
Preprint. Discussion started: 21 March 2025

$DAOD$), I find nonsignificant AODNOD increases for global and extratropical land, but significant increases over tropical land at 2.35 ± 2.33 10^{-3} (5 of 8 models agree on this increase).

Of the three models with an interactive representation of BVOCs, only two archived AOD (GFDL-ESM4 and UKESM1-0-LL), and both models yield much larger AOD increases than the other models. Such AOD increases are consistent with enhanced BVOC emissions due to the increased vegetation (e.g., LAI; Fig. 1b), leading to more secondary organic aerosol (e.g., Scott et al., 2018; Weber et al., 2024). For example, AOD increases over global land by 7.78 ± 1.00 10^{-3} and 7.87 ± 0.78 10^{-3} for GFDL-ESM4 and UKESM1-0-LL, respectively (compared to the multimodel mean increase of 1.88 ± 2.50 10^{-3}). For GFDL-ESM4, a large fraction of this AOD increase is due to an increase in DAOD at 4.82 ± 0.91 10^{-3} (UKESM1-0-LL yields a nonsignificant DAOD decrease of -0.38 ± 0.78 10^{-3}). Nonetheless, AODNOD (which includes SOA) yields relatively large and significant global land increases for both models at 2.97 ± 0.41 10^{-3} for GFDL-ESM4 and 8.26 ± 0.38 10^{-3} for UKESM1-0-LL (Supplementary Figure 7g-h). These values increase over tropical land (where vegetation indices also increase the most) at 6.16 ± 0.85 10^{-3} and 10.68 ± 0.63 10^{-3} for GFDL-ESM4 and UKESM1-0-LL, respectively. In turn, both models feature SW_{clear} SEB cooling (consistent with enhanced aerosol scattering) over global land (and over tropical and extratropical land) of -0.13 ± 0.02 for GFDL-ESM4 and -0.07 ± 0.02 K for UKESM1-0-LL (compared to the multimodel mean of -0.05 ± 0.02 K). NorESM2-LM, the other model with an interactive representation of BVOCs (but no AOD data), also yields relatively large SW_{clear} SEB cooling at -0.08 ± 0.03 K. The GFDL-ESM4 SW_{clear} cooling is the second largest of the 15 models; the NorESM2-LM and UKESM1-0-LL SW_{clear} cooling are third and fourth largest, respectively. Similar statements also generally apply for tropical land, e.g., the NorESM2-LM SW_{clear} cooling of -0.16 ± 0.05 K is the largest and the GFDL-ESM4 SW_{clear} cooling of -0.11 ± 0.03 K is the third largest; however, UKESM1-0-LL SW_{clear} cooling is not exceptional at -0.04 ± 0.04 K (compared to the multimodel mean of -0.05 ± 0.02 K). Thus, consistent with Gomez et al. (2023), there is evidence that models with interactive chemistry yield AOD increases under carbon fertilization, consistent with enhanced vegetation leading to more BVOC emissions and SOA. In turn, this appears to strengthen the cooling associated with the SW_{clear} SEB term (with enhanced water vapor and reduced surface solar radiation also contributing). I also note that the AOD increase here is also consistent with the land-sea warming contrast (e.g., Fig. 2a) and reduced precipitation over land (Supplementary Figure 5b), which leads to less aerosol wet removal (Allen et al., 2019).

As the SW_{clear} SEB term leads to multimodel mean cooling, the warming under the (total) SW SEB term is therefore associated with clouds. SW_{cloud} yields multimodel mean global land warming of 0.14 ± 0.05 K (12 of 15 models agree on the increase), which increases to 0.21 ± 0.08 K over extratropical land. As with the LW_{cloud} SEB cooling, this SW_{cloud} SEB warming is consistent with decreases in cloud cover (e.g., here, less cloud cover will lead to enhanced surface solar radiation and warming). Moreover, both the LW_{cloud} and SW_{cloud} SEB terms are largest in magnitude in the extratropics, consistent with larger extratropical cloud cover decrease. I note that the net effect of clouds is controlled by their impact on shortwave as opposed to longwave radiation. The SW_{cloud} SEB term yields multimodel global land mean warming of 0.14 ± 0.05 K, while the LW_{cloud} SEB term yields corresponding cooling of -0.07 ± 0.03 K. This implies the net effect of clouds is associated with warming of 0.07 ± 0.06 K. The net warming effect from clouds increases over extratropical land at 0.10 ± 0.09 K.

https://doi.org/10.5194/egusphere-2025-32
Preprint. Discussion started: 21 March 2025

I also note that I do not find evidence for an aerosol indirect effect on clouds and in turn the SW_{cloud} SEB term. As discussed above, the two models with interactive chemistry simulate relatively large and significant increases in AODNOD, particularly over tropical land (which potentially leads to SW_{cloud} cooling related to cloud brightening and enhanced cloud lifetime). However, as with the multimodel mean, SW_{cloud} leads to warming over global land, tropical land and extratropical land for both models (as well as NorESM2-LM). UKESM1-0-LL actually yields the largest SW_{cloud} warming of the 15 models over both global land and tropical land at 0.32 ± 0.02 K and 0.28 ± 0.05 K, respectively. In contrast to an aerosol indirect effect, this SW_{cloud} warming in UKESM1-0-LL is consistent with a decrease in cloud cover, as UKESM1-0-LL yields the second largest cloud cover decrease over global land at -1.35 ± 0.14% and the third largest decrease over tropical land at -1.20 ± 0.29%. Overall, the (total) SW SEB term warms global land in UKESM1-0-LL and NorESM2-LM by 0.25 ± 0.03 K and 0.10 ± 0.05 K, respectively, with nonsignificant cooling of -0.02 ± 0.02 K for GFDL-ESM4. Thus, as with the multimodel mean results, SW_{cloud} SEB warming dominates over SW_{clear} SEB cooling in these three models. Any impacts of interactive chemistry and enhanced BVOC emissions/SOA on clouds appear to be minor in these simulations and do not lead to an appreciable increase in cooling.

Spatially correlating the multimodel mean SEB responses with the corresponding total SEB response yields significant global (land only) correlations for all individual SEB terms (Supplementary Table 5). Consistent with the sign of the multimodel mean SEB responses, the total SEB term is positively correlated with the surface albedo, SW, SW_{cloud}, LW, LW_{clear}, LH and canopy transpiration SEB terms. Similarly, the total SEB term is negatively correlated with the SW_{clear}, LW_{cloud}, SH and evaporation SEB terms. The LW_{clear} SEB term yields the largest global correlation with the total SEB term at 0.91. This very high correlation adds additional evidence that the LW_{clear} SEB term is largely a feedback to the surface warming. Restricting this analysis to the tropics yields maximum correlations between the total SEB term and the LH SEB term at 0.77, followed closely by the LW_{clear} SEB term at 0.76. This provides additional support for the importance of the multimodel mean LH SEB response to the total SEB response in the tropics. In the extratropics, maximum correlations occur for LW_{clear} at 0.90, followed by LW at 0.58 and SW_{cloud} at 0.57.

I conduct additional analyses to better understand causes of inter-model spread in the SEB responses. Supplementary Figures 8 and 9 shows spatial correlations (across models) between the total SEB term and each of the SEB components. The LW SEB term show very large and significant correlations ($r > 0.80$) throughout most of the Northern Hemisphere (with nearly all land areas exhibiting similarly large and significant correlations under LW_{clear}). The LH SEB term shows relatively large and significant positive correlations ($r > 0.70$) throughout the tropics (minus the Sahara Desert). The surface albedo SEB term shows relatively large and significant positive correlations ($r > 0.70$) in the NH extratropics. This suggests much of the intermodel variation in the total SEB extratropical surface temperature response is related to intermodel differences in the SEB surface albedo term response; in the tropics, intermodel variation in the total SEB tropical surface temperature response is related to intermodel differences in the SEB surface LH term response.

https://doi.org/10.5194/egusphere-2025-32
Preprint. Discussion started: 21 March 2025

These broad conclusions are consistent with Supplementary Figures 10-15, which show corresponding model scatterplots between the total SEB term and its components for the global land mean (Supplementary Figures 10-11), tropical land mean (Supplementary Figures 12-13) and extratropical land mean (Supplementary Figures 14-15). The sign of all of the intermodel correlations is consistent with the multimodel mean responses, i.e., positive intermodel correlations (although many are not significant) between the total SEB response and the SEB albedo, SW, LW, and LH responses occur. Similarly, a negative correlation between the total SEB response and the SEB SH response occurs. A similar statement can be made for the additional SEB terms where positive correlations exist between the total SEB term and the SW_{cloud}, LW_{clear}, and canopy transpiration SEB terms, with negative correlations for the SW_{clear} (except for the tropics), LW_{cloud} and evpoaration SEB terms. Globally (Supplementary Figures 10-11), the intermodel variation in the total SEB response is largely related to the intermodel variation in the SEB albedo response, with a correlation of 0.73 (significant at the 99% confidence level). As noted above, CNRM-ESM2-1 is the lone model that yields significant surface cooling (e.g., Supp. Fig. 2f) and this is the lone model that yields cooling for the SEB albedo term. Furthermore, as noted above UKESM1-0-LL and EC-Earth3-CC yield relative large total SEB warming, and they both possess relatively large SEB surface albedo warming. The LW SEB term also yields a similar correlation at 0.73, which improves to 0.86 for LW_{clear}. As noted above, however, I suggest this is largely a response to the warming and not a primary driver. Interestingly, the correlation between the LH SEB term and the total SEB term is not significant at 0.13. The lone model that yields cooling for the LH SEB term is EC-Earth3-CC, and this is a model with relatively large total SEB warming. This implies intermodel variation in the relative importance of the individual SEB responses their total SEB response.

In the tropics, the intermodel variation in the total SEB term is largely related to the SW SEB term with a correlation of 0.70 (99%), which is largely due to SW_{cloud} (r=0.74). The LH SEB term is also important with a correlation at 0.54 (95%). In the extratropics, the intermodel variation in the total SEB term is largely related to the SEB albedo term with a correlation of 0.81 (99%). The LW SEB term also yields a similar correlation at 0.79, which improves to 0.91 for LW_{clear}.

Finally, I note a significant correlation of 0.55 (significant at the 95% confidence level; Figure 5) between the transient climate response (TCR; warming centered on the time of CO_2 doubling) and the global mean biogeophyscial temperature response associated with carbon fertilization across models. The correlation improves to 0.68 (significant at the 99% confidence level) over global land only (Fig. 5b). In other words, models with a larger (smaller) TCR tend to have larger (smaller) biogeophysical warming under carbon fertilization. This is not necessarily unexpected, since the TCR is based on the $1PCTCO_2$ experiments, which include the $1PCTCO_2$-bgc responses. Moreover, the causes of larger TCR (e.g., climate feedbacks including water vapor, tropospheric lapse rate, surface albedo and clouds) also operate in the $1PCTCO_2$-bgc runs. In particular, the three models (EC-Earth3-CC, UKESM1-0-LL and CESM2) mentioned above that yield the largest biogeophysical warming associated with carbon fertilization are among the models with the largest TCR (CanESM5 is an exception at it has a large TCR but relatively small biogeophysical warming). On one hand, this implies the intermodel spread in the biogeophysical warming associated with carbon fertilization is related to the TCR; on the other hand, it also implies the importance of the biogeophysical warming associated with the carbon fertilization

https://doi.org/10.5194/egusphere-2025-32
Preprint. Discussion started: 21 March 2025

effect to intermodel variation in the TCR. I reiterate, however, that the magnitude of biogeophysical warming associated with carbon fertilization is relatively small. If I re-estimate the global mean near surface air temperature response over the time of CO_2 doubling (years 60-79, as with TCR), I find biogeophysical warming of 0.12 ± 0.08 K, i.e., about 6% as large as the multimodel mean TCR of 1.97 ± 0.20 K. However, some models yield much larger biogeophysical warming at the time of CO_2 doubling, including many of the same models previously discussed. EC-Earth3-CC yields warming of 0.26 ± 0.05 K, which is 10% of its TCR of 2.7 ± 0.10 K. CESM2 yields warming of 0.49 ± 0.07 K, which is 20% of its TCR of 2.4 ± 0.07 K. UKESM1-0-LL yields a percentage closer to the multimodel mean, with warming of 0.19 ± 0.07 K, which is 7% of its TCR of 2.7 ± 0.14 K. Additional discussion on potential causes of intermodel differences is included in the Supplement (Supplementary Note 1).

4. Conclusions

Using 15 CMIP6 models, I show that carbon fertilization at the time of CO_2 quadrupling (and in the absence of radiative warming from CO_2) yields biogeophysical global mean warming of 0.16 ± 0.09 K with 13 of the 15 models yielding warming. This warming increases over global land to 0.28 ± 0.13 K with 14 of the 15 models yielding warming (Supplementary Table 4). Using the surface energy balance decomposition to understand the drivers of this warming shows that it is largely related to decreased latent heat flux, which leads to global land warming of 0.27 ± 0.11 K (13 of 15 models agree on the warming). This in turn is largely associated with reduced canopy transpiration which leads to global land warming of 0.45 ± 0.15 (13 of 13 models agree on the warming). Such a response is consistent with reduced stomatal conductance under elevated CO_2 (e.g., Wong et al., 1979; Keenan et al., 2013). To some extent, this warming if offset by increases in evaporation, which leads to global land cooling of -0.19 ± 0.16 K. This cooling, however, is less robustly simulated with only 9 of the 13 models agreeing on the cooling. In the tropics, the importance of transpiration induced warming increases to 0.70 ± 0.26 K (13/13 models agree). Tropical land evaporation increases only marginally to -0.26 ± 0.25 K but with limited model agreement (7/13 models agree on the cooling). Of the various SEB terms, the evaporation term is the most uncertain across the models (particularly in the tropics) with limited model agreement on the sign of the response. Given the importance of LH to the biogeophysical warming response (both its direct impact as well as its indirect impact on clouds and subsequently LW_{cloud} and SW_{cloud}) and the competing effects of transpiration versus evaporation, the low model agreement on the sign of the evaporation response highlights an important source of model uncertainty.

Other important drivers of biogeophysical warming under carbon fertilization, particularly in the extratropics, include reduced albedo and enhanced SW radiation due to a decrease in cloud cover. Warming due to reduced albedo is consistent with the surface darkening effect of vegetation (e.g., Betts et al., 2000, Bala et al., 2006; Li et al., 2015), particularly at higher latitudes where snow/ice is more prevalent. Warming due to enhanced shortwave radiation due to clouds is consistent with decreases in total cloud cover. Similar to the decrease in latent heat flux, the decrease in cloud cover is related to the reduced stomatal conductance, which is associated with reduced relative humidity over land which promotes a decrease in cloud cover. Models with interactive BVOCs yield a larger increase in AOD, which strengthens the cooling associated with the SW_{clear}; however, as with the multimodel mean, SW_{cloud} warming dominates

https://doi.org/10.5194/egusphere-2025-32
Preprint. Discussion started: 21 March 2025

over SW_{clear} cooling in these models, implying any aerosol effect is minor in these simulations (i.e., the dominant SW effect is warming due to cloud cover reductions associated with decreases in transpiration).

Intermodel variation in the vegetation and biogeophysical temperature responses was also evaluated. Although there are significant differences between models with and without a terrestrial nitrogen cycle (e.g., N models yields significantly less carbon storage), most of these differences (e.g., N models tend to yield less biogeochemical cooling) are not significant. However, intermodel biogeophysical warming significantly correlates with each model's TCR. This implies the causes of intermodel TCR variation (i.e., climate feedbacks) are also responsible for some of the intermodel spread in the biogeophysical temperature response under carbon fertilization. Finally, the increase in land carbon storage under carbon fertilization was used to estimate the biogeochemical cooling effect using the transient climate response to cumulative emissions. I find that biogeochemical cooling of −1.38 K (−1.92 to −0.84 K) dominates over biogeophysical warming, by about an order of magnitude.

Code Availability
Standard code (e.g., NCL) was used to analyze the model simulations.

Data Availability
CMIP6 data can be downloaded from the Earth System Grid Federation at https://aims2.llnl.gov/search.

Author Contributions
RJA conceived the project, analyzed model simulations and wrote the manuscript.

Competing Interests
The author declares no competing interests.

Acknowledgements
R. J. Allen is supported by NSF grant AGS-2153486.

Financial Support
This research has been supported by the National Science Foundation (grant no. AGS-2153486).

References

Ainsworth, E. A. and Rogers, A. The response of photosynthesis and stomatal conductance to rising [CO2]: mechanisms and environmental interactions. *Plant Cell Environ*. **30** (3), 258-270 (2007). doi: 10.1111/j.1365-3040.2007.01641.x.

Ainsworth, E. A. and Long, S. P. What have we learned from 15 years of free-air CO_2 enrichment (FACE)? A meta-analytic review of the responses of photosynthesis, canopy properties and plant production to rising CO_2. *New Phytologist*, **165**, 351-372, (2005). doi: 10.1111/j.1469-8137.2004.01224.x.

Allen, R. J., Gomez, J., Horowitz, L. W. and Shevliakova E. Enhanced future vegetation growth with elevated carbon dioxide concentrations could increase fire activity. *Commun Earth Environ* **5**, 54 (2024). doi: 10.1038/s43247-024-01228-7.

Allen, R. J., Hassan, T. Randles, C. A. and Su, H. Enhanced land–sea warming contrast elevates aerosol pollution in a warmer world. *Nat. Clim. Chang.* **9**, 300–305 (2019). doi: 10.1038/s41558-019-0401-4.

Arora, V. K., Katavouta, A., Williams, R. G., Jones, C. D., Brovkin, V., Friedlingstein, P., Schwinger, J., Bopp, L., Boucher, O., Cadule, P., Chamberlain, M. A., Christian, J. R., Delire, C., Fisher, R. A., Hajima, T., Ilyina, T., Joetzjer, E., Kawamiya, M., Koven, C. D., Krasting, J. P., Law, R. M., Lawrence, D. M., Lenton, A., Lindsay, K., Pongratz, J., Raddatz, T., Séférian, R., Tachiiri, K., Tjiputra, J. F., Wiltshire, A., Wu, T., and Ziehn, T. Carbon–concentration and carbon–climate feedbacks in CMIP6 models and their comparison to CMIP5 models, *Biogeosciences*, **17**, 4173–4222, (2020). doi: 10.5194/bg-17-4173-2020.

Bala, G., Caldeira, K., Mirin, A., Wickett, M., Delire, C. and Phillips, T. J. Biogeophysical effects of CO_2 fertilization on global climate. *Tellus B*, **58**, 620-627, (2006). doi: 10.1111/j.1600-0889.2006.00210.x.

Betts, R. A. Offset of the potential carbon sink from boreal forestation by decreases in surface albedo. *Nature*, **408**, 187-190, (2000). doi: 10.1038/35041545.

Bounoua, L., Collatz, G. J., Sellers, P. J., Randall, D. A., Dazlich, D. A., Los, S. O., Berry, J. A., Fung, I., Tucker, C. J., Field, C. B. and Jensen, T. G. Interactions between Vegetation and Climate: Radiative and Physiological Effects of Doubled Atmospheric CO2. *J. Climate*, **12**, 309–324, (1999). doi: 10.1175/1520-0442(1999)012<0309:IBVACR>2.0.CO;2.

Boysen, L. R., Brovkin, V., Pongratz, J., Lawrence, D. M., Lawrence, P., Vuichard, N., Peylin, P., Liddicoat, S., Hajima, T., Zhang, Y., Rocher, M., Delire, C., Séférian, R., Arora, V. K., Nieradzik, L., Anthoni, P., Thiery, W., Laguë, M. M., Lawrence, D., and Lo, M.-H. Global climate response to idealized deforestation in CMIP6 models. *Biogeosciences*, *17*, 5615-5638 (2020). doi: 10.5194/bg-17-5615-2020.

Campbell, J., Berry, J., Seibt, U., Smith, S. J., Montzka, S. A., Launois, T., Belviso, S., Bopp, L. and Laine, M. Large historical growth in global terrestrial gross primary production. *Nature* **544**, 84–87 (2017). doi: 10.1038/nature22030.

Canadell, J.G., P.M.S. Monteiro, M.H. Costa, L. Cotrim da Cunha, P.M. Cox, A.V. Eliseev, S. Henson, M. Ishii, S. Jaccard, C. Koven, A. Lohila, P.K. Patra, S. Piao, J. Rogelj, S. Syampungani, S. Zaehle, and K. Zickfeld, 2021: Global Carbon and other Biogeochemical Cycles and Feedbacks. In Climate Change 2021: The Physical Science Basis. Contribution of Working Group I to the Sixth Assessment Report of the Intergovernmental Panel on Climate Change [Masson-Delmotte, V., P. Zhai, A. Pirani, S.L. Connors, C. Péan, S. Berger, N. Caud, Y. Chen, L. Goldfarb, M.I. Gomis, M. Huang, K. Leitzell, E. Lonnoy, J.B.R. Matthews, T.K. Maycock, T. Waterfield, O. Yelekçi, R. Yu, and B. Zhou (eds.)]. Cambridge University Press, Cambridge, United Kingdom and New York, NY, USA, pp. 673–816, doi:10.1017/9781009157896.007.

Cao, L., Bala, G., Caldeira, K., Nemani, R. and Ban-Weiss, G. Importance of carbon dioxide physiological forcing to future climate change. *Proc. Natl. Acad. Sci. U.S.A.*, **107** (21), 9513-9518, (2010). doi: 10.1073/pnas.0913000107.

Chen, C., Riley, W. J., Prentice, I. C. and Keenan, T. F. CO2 fertilization of terrestrial photosynthesis inferred from site to global scales. *Proc. Natl Acad. Sci. USA* **119** (10), e2115627119, (2022). doi: 10.1073/pnas.2115627119.

Doutriaux-Boucher, M., Webb, M. J., Gregory, J. M. and Boucher, O. Carbon dioxide induced stomatal closure increases radiative forcing via a rapid reduction in low cloud, *Geophys. Res. Lett.*, **36**, L02703, (2009). doi:10.1029/2008GL036273.

Eyring, V., Bony, S., Meehl, G. A., Senior, C. A., Stevens, B., Stouffer, R. J., and Taylor, K. E. Overview of the Coupled Model Intercomparison Project Phase 6 (CMIP6) experimental design and organization. *Geosci. Model Dev.*, **9**, 1937–1958, (2016). doi: 10.5194/gmd-9-1937-2016.

Fernández-Martínez, M., Vicca, S., Janssens, I. A., Sardans, J., Luyssaert, S., Campioli, M., Chapin, F. S. III, Ciais, P., Malhi, Y., Obersteiner, M., Dapale, D., Piao, S. L., Reichstein, M., Roda, F. and Penuelas, J. Nutrient availability as the key regulator of global forest carbon balance. *Nature Clim Change* **4**, 471–476 (2014). doi: 10.1038/nclimate2177.

Field, C. B., Jackson, R. B. and Mooney H. A. Stomatal responses to increased CO_2: implications from the plant to the global scale. *Plant, Cell & Environment*, **18**, 1214-1225 (1995). doi: 10.1111/j.1365-3040.1995.tb00630.x.

Forkel, M., Carvalhais, N., Rodenbeck, C., Keeling, R., Heimann, M., Thonicke, K., Zaehle, S. and Reichstein, M. Enhanced seasonal CO_2 exchange caused by amplified plant productivity in northern ecosystems. *Science,* **351**, 696-699 (2016). doi:10.1126/science.aac4971.

Gier, B. K., Schlund, M., Friedlingstein, P., Jones, C. D., Jones, C., Zaehle, S., and Eyring, V.

https://doi.org/10.5194/egusphere-2025-32
Preprint. Discussion started: 21 March 2025

Representation of the terrestrial carbon cycle in CMIP6, *Biogeosciences*, **21**, 5321–5360, (2024). doi: 10.5194/bg-21-5321-2024.

Gillett, N. P., Arora,V. K., Matthews, D. and Allen, M. R. Constraining the Ratio of Global Warming to Cumulative CO_2 Emissions Using CMIP5 Simulations, *J. Climate*, **26**, 6844–6858, (2013). doi: 10.1175/JCLI-D-12-00476.1.

Gomez, J., Allen, R. J., Turnock, S. T., Horowitz, L. W., Tsigaridis, K., Bauer, S. E., Olivie, D., Thomson, E. S. and Ginoux, P. The projected future degradation in air quality is caused by more abundant natural aerosols in a warmer world. *Commun Earth Environ* **4**, 22 (2023). doi: 10.1038/s43247-023-00688-7.

Haverd, V., Smith, B., Canadell, J. G., Cuntz, M., Mikaloff-Fletcher, S., Garquhar, G., Woodgate, W., Briggs, P. R., and Trudinger, C. M. Higher than expected CO_2 fertilization inferred from leaf to global observations. *Glob Chang Biol*. **26** (4), 2390-2402, (2020). doi: 10.1111/gcb.14950.

Hirsch, A. L., Guillod, B. P., Seneviratne, S. I., Beyerle, U., Boysen, L. R., Brovkin, V., Davin, E. L., Doelman, J. C., Kim, H., Mitchell, D. M., Nitta, T., Shiogama, H., Sparrow, S., Stehfest, E., van Vuuren, D. P., and Wilson, S. Biogeophysical Impacts of Land-Use Change on Climate Extremes in Low-Emission Scenarios: Results From HAPPI-Land, *Earth's Future*, **6**, 396–409 (2018). doi: 10.1002/2017EF000744.

Jones, C. D., Arora, V., Friedlingstein, P., Bopp, L., Brovkin, V., Dunne, J., Graven, H., Hoffman, F., Ilyina, T., John, J. G., Jung, M., Kawamiya, M., Koven, C., Pongratz, J., Raddatz, T., Randerson, J. T., and Zaehle, S. C4MIP – The Coupled Climate–Carbon Cycle Model Intercomparison Project: experimental protocol for CMIP6, *Geosci. Model Dev*., **9**, 2853–2880, (2016). doi: 10.5194/gmd-9-2853-2016,

Keeling, R. F., Graven, H. D., Welp, L. R., Resplandy, L., Bi, J., Piper, S. C., Sun, Y., Bollenbacher, A. and Meijer, H. A. J. Atmospheric evidence for a global secular increase in carbon isotopic discrimination of land photosynthesis, *Proc. Natl. Acad. Sci. U.S.A.* **114**, (39), 10361-10366, (2017). doi: 10.1073/pnas.1619240114.

Keenan, T. F., Hollinger, D. Y., Bohrer, G., Dragoni, D., William Munger, J., Schmid, H. P. and Richardson, A. D. Increase in forest water-use efficiency as atmospheric carbon dioxide concentrations rise. *Nature*, **499**, 324–327, (2013).

Keenan, T. F., Luo, X., Stocker, B. D., De Kauwe, M. G., Medlyn, B. E., Prentice, I. C., Smith, N. G., Terrer, C., Wang, H., Zhang, Y. and Zhou, S. A constraint on historic growth in global photosynthesis due to rising CO_2. *Nat. Clim. Chang.* **13**, 1376–1381 (2023). doi: 10.1038/s41558-023-01867-2.

Kicklighter, D.W., Melillo, J. M., Monier, E., Sokolov, A. P. and Zhuang, Q. Future nitrogen availability and its effect on carbon sequestration in Northern Eurasia. *Nat. Commun.* **10**, 3024 (2019). doi: 10.1038/s41467-019-10944-0.

Leakey, A. D., Ainsworth, E. A., Bernacchi, C. J., Rogers, A., Long, S. P. and Ort, D. R. Elevated CO_2 effects on plant carbon, nitrogen, and water relations: Six important lessons from FACE. *Journal of Experimental Botany*, **60**(10), 2859-2876, (2009). doi: 10.1093/jxb/erp096.

Li, Y., Zhao, M., Motesharrei, S., Mu, Q., Kalnay, E. and Li, S. Local cooling and warming effects of forests based on satellite observations. *Nat Commun.* **6**, 6603, (2015). doi: 10.1038/ncomms7603.

Luyssaert, S., Jammet, M., Stoy, P. C., Estel, S., Pongratz, J., Ceschia, E., Churkina, G., Don, A., Erb, K., Ferlicoq, M., Gielen, B., Grünwald, T., Houghton, R. A., Klumpp, K., Knohl, A., Kolb, T., Kuemmerle, T., Laurila, T., Lohila, A., Loustau, D., McGrath, M. J., Meyfroidt, P. Moors, E. J., Naudts, K., Novick, K., Otto, J., Pilegaard, K., Pio, C. A., Rambal, S., Rebmann, C., Ryder, J., Suyker, A. E., Varlagin, A., Wattenbach, M., and Dolman, A. J. Land management and land-cover change have impacts of similar magnitude on surface temperature. *Nat. Clim. Change*, **4**, 389–393, (2014). doi: 10.1038/nclimate2196.

Norby, R. J., and Zak. D. R. Ecological lessons from Free-Air CO_2 Enrichment (FACE) experiments. *Annual Review of Ecology, Evolution, and Systematics*, **42**(1), 181-203, (2011). doi: 10.1146/annurev-ecolsys-102209-144647.

Oren, R., Ellsworth, D. S., Johnsen, K. H., Phillips, N., Ewers, B. E., Maier, C., Schafer, K., McCarthy, H., Hendrey, G., McNulty, S. G., and Katul, G. G. Soil fertility limits carbon sequestration by forest ecosystems in a CO_2-enriched atmosphere. *Nature* **411**, 469–472 (2001). doi: 10.1038/35078064.

Scott, C. E., Monks, S. A., Spracklen, D. V., Arnold, S. R., Forster, P. M., Rap, A., Aijala, M., Artaxo, P., Carslaw, K. S., Chipperfield, M. P., Ehn, M., Gilardoni, S., Heikkinen, L., Kulmala, M., Peraja, T., Reddington, C. L. S., Rizzo, L. V., Swietlicki, E., Vignati, E. amd Wilson, C. Impact on short-lived climate forcers increases projected warming due to deforestation. *Nat Commun* **9**, 157 (2018). doi: 10.1038/s41467-017-02412-4.

Thomas, R. T., Prentice, I. C., Graven, H., Ciais, P., Fisher, J. B., Hayes, D. J., Huang, M., Huntzinger, D. N., Ito, A., Jain, A., Mao, J., Michalak, A. M., Peng, S., Poulter, B., Ricciuto, D. M., Shi, X., Schwalm, C., Tian, H. and Zeng, N. Increased light-use efficiency in northern terrestrial ecosystems indicated by CO_2 and greening observations. *Geophys. Res. Lett.*, **43**, 11,339–11,349, (2016). doi:10.1002/2016GL070710.

Vargas Zeppetello, L. R., Donohoe, A. and Battisti, D. S. Does surface temperature respond to or determine downwelling longwave radiation? *Geophysical Research Letters*, **46**, 2781–2789 (2019). doi: 10.1029/2019GL082220.

Vitousek, P.M. and Howarth, R. W.. Nitrogen limitation on land and in the sea: How can it occur?. *Biogeochemistry* **13**, 87–115 (1991). doi: 10.1007/BF00002772.

https://doi.org/10.5194/egusphere-2025-32
Preprint. Discussion started: 21 March 2025

Walker, A.P., De Kauwe, M.G., Bastos, A., Belmecheri, S., Georgiou, K., Keeling, R.F., McMahon, S.M., Medlyn, B.E., Moore, D.J.P., Norby, R.J., Zaehle, S., Anderson-Teixeira, K.J., Battipaglia, G., Brienen, R.J.W., Cabugao, K.G., Cailleret, M., Campbell, E., Canadell, J.G., Ciais, P., Craig, M.E., Ellsworth, D.S., Farquhar, G.D., Fatichi, S., Fisher, J.B., Frank, D.C., Graven, H., Gu, L., Haverd, V., Heilman, K., Heimann, M., Hungate, B.A., Iversen, C.M., Joos, F., Jiang, M., Keenan, T.F., Knauer, J., Körner, C., Leshyk, V.O., Leuzinger, S., Liu, Y., MacBean, N., Malhi, Y., McVicar, T.R., Penuelas, J., Pongratz, J., Powell, A.S., Riutta, T., Sabot, M.E.B., Schleucher, J., Sitch, S., Smith, W.K., Sulman, B., Taylor, B., Terrer, C., Torn, M.S., Treseder, K.K., Trugman, A.T., Trumbore, S.E., van Mantgem, P.J., Voelker, S.L., Whelan, M.E. and Zuidema, P.A. Integrating the evidence for a terrestrial carbon sink caused by increasing atmospheric CO_2. *New Phytol.*, **229**, 2413-2445, (2021). doi: 10.1111/nph.16866.

Weber, J., King, J. A., Abraham, N. L., Grosvenor, J. P., Smith, C. J., Shin, Y. M., Lawrence, P., Roe, S., Beerling, D. J. and Val Martin, V. Chemistry-albedo feedbacks offset up to a third of forestation's CO2 removal benefits. *Science* **303** (6685), 860-864 (2024). doi: 10.1126/science.adg6196.

Wong, S. C., Cowan, I. R. and Farquhar, G. D. Stomatal conductance correlates with photosynthetic capacity. *Nature*, **282**, 424–426, (1979).

Zhu, Z., Piao, S., Myneni, R. B., Huang, M., Zeng, Z., Canadell, J. G., Ciais, P., Sitch, S., Friedlingstein, P., Arneth, A., Cao, C., Cheng, L., Kato, E., Koven, C., Li, Y., Lian, X., Liu, Y., Liu, R., Mao, J., Pan, Y., Peng, S., Peñuelas, J., Poulter, B., Pugh, T. A. M., Stocker, B. D., Viovy, N., Wang, X., Wang, Y., and Xiao, Z., Yang, H., Zaehle, S. and Zeng, N. Greening of the Earth and its drivers. *Nat. Clim. Change* **6**, 791–795 (2016). doi: 10.1038/nclimate3004.

https://doi.org/10.5194/egusphere-2025-32
Preprint. Discussion started: 21 March 2025

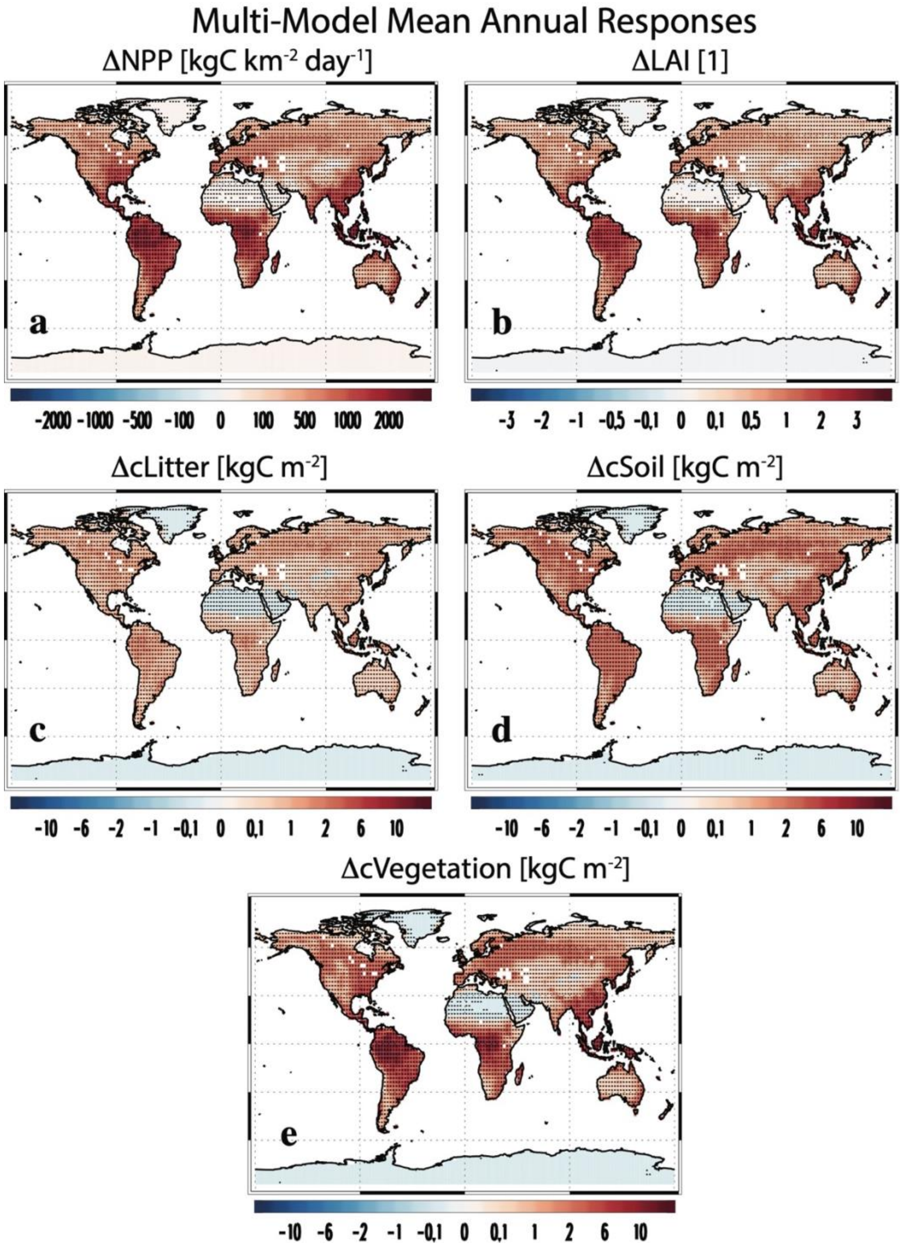

Figure 1. Vegetation and land carbon responses. Multimodel mean annual mean responses for (a) net primary productivity (NPP; kgC km^{-2} day^{-1}); (b) leaf area index (LAI; dimensionless); (c) litter pool carbon (cLitter; kgC m^{-2}); (d) soil pool carbon (cSoil; kgC m^{-2}); and (e) vegetation carbon (cVegetation; kgC m^{-2}). Symbols denote a response significant at the 90% confidence level based on a two-tailed pooled t-test.

https://doi.org/10.5194/egusphere-2025-32
Preprint. Discussion started: 21 March 2025

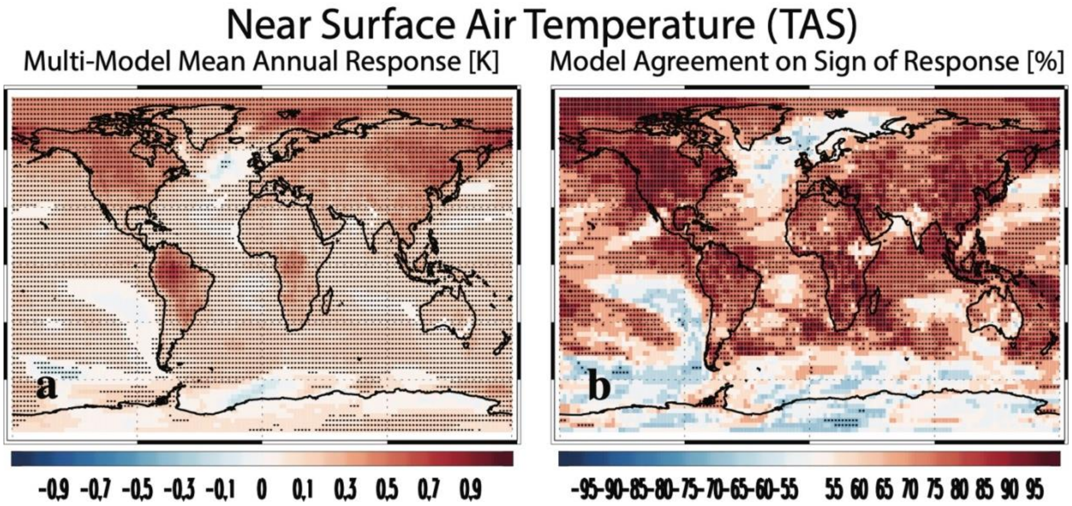

Figure 2. Near surface air temperature. (a) Multimodel mean annual mean near surface air temperature (TAS; K) response. Symbols denote a response significant at the 90% confidence level based on a two-tailed pooled t-test. (b) Model agreement on the sign of the TAS response [% of models]. Red (blue) colors indicate model agreement on an increase (decrease). Symbols represent significant model agreement at the 90% confidence level based on a two-tailed binomial test.

https://doi.org/10.5194/egusphere-2025-32
Preprint. Discussion started: 21 March 2025

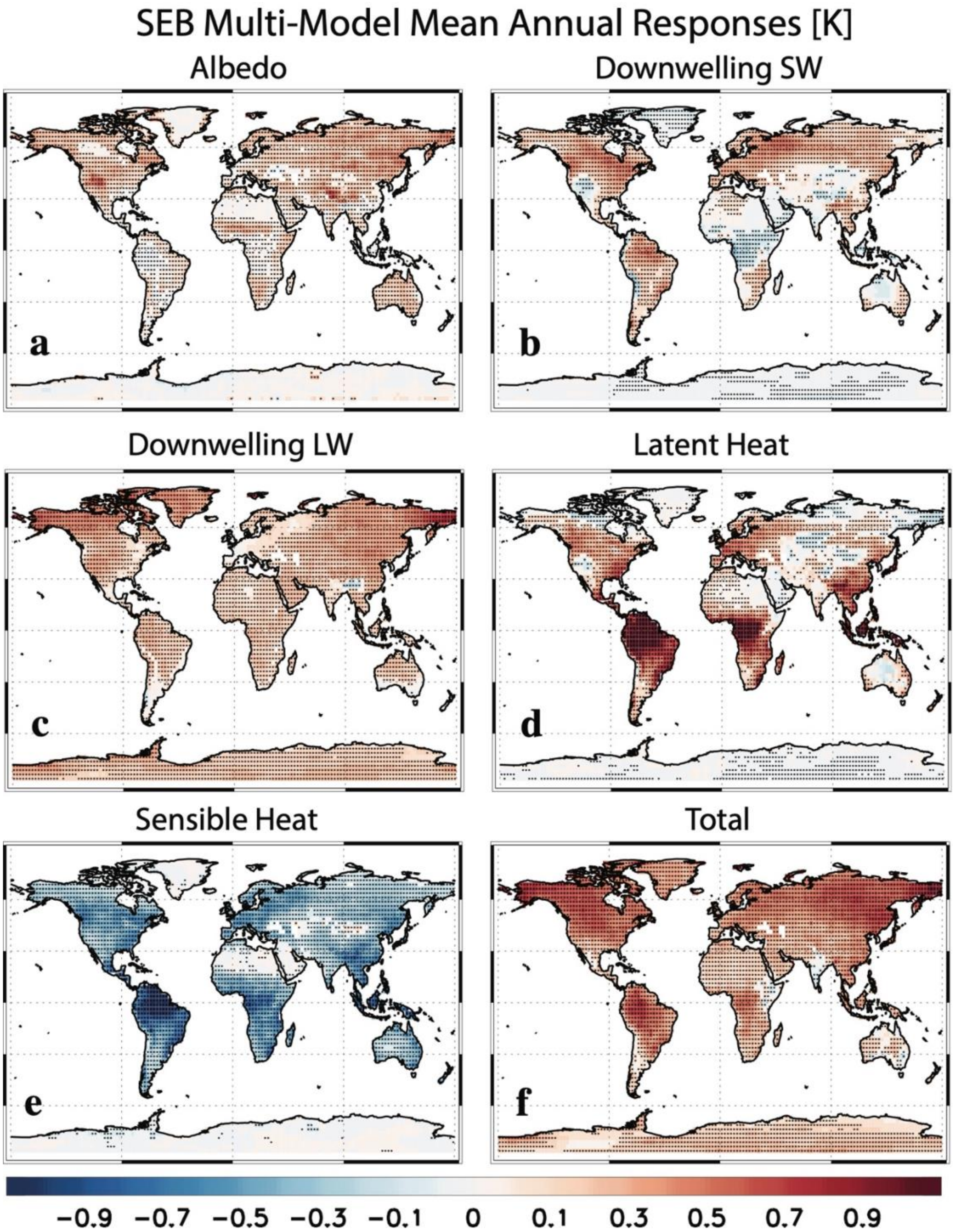

Figure 3. Surface energy balance (SEB) decomposition of the surface temperature response. Multimodel mean annual mean SEB responses for (a) surface albedo; (b) downwelling surface shortwave radiation; (c) downwelling surface longwave radiation; (d) surface latent heat flux; (e) surface sensible heat flux; and (f) the total (i.e., sum of the prior five terms). Units are K. Symbols denote a response significant at the 90% confidence level based on a two-tailed pooled t-test.

https://doi.org/10.5194/egusphere-2025-32
Preprint. Discussion started: 21 March 2025

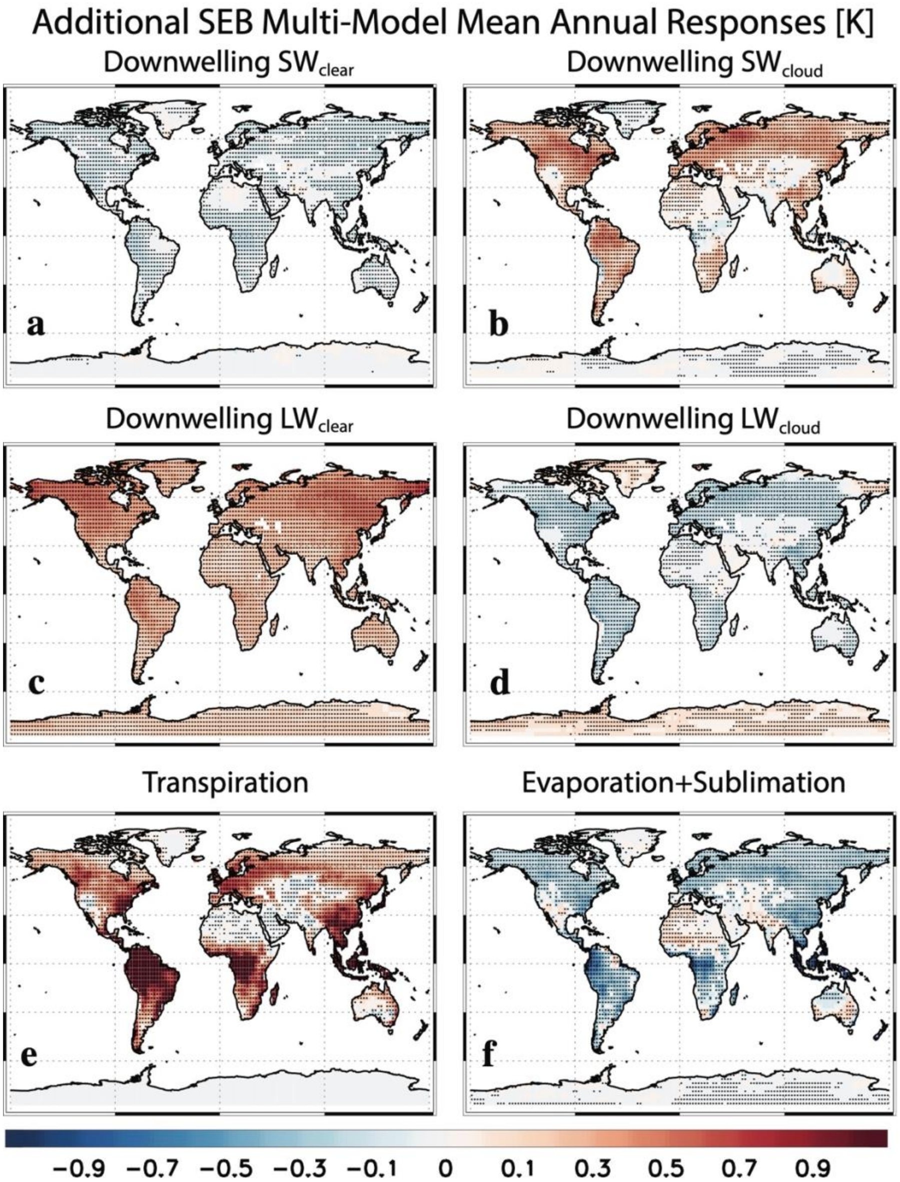

Figure 4. Additional surface energy balance (SEB) decomposition of the surface temperature response. Multimodel mean annual mean SEB responses for downwelling surface shortwave radiation decomposed into (a) clear-sky (SW_{clear}) and (b) cloudy-sky (SW_{cloud}) contributions; downwelling surface longwave radiation decomposed into (c) clear-sky (LW_{clear}) and (d) cloudy-sky (LW_{cloud}) contributions; and surface latent heat flux decomposed into (e) canopy transpiration and (f) evaporation (which includes sublimation) contributions. Units are K. Symbols denote a response significant at the 90% confidence level based on a two-tailed pooled t-test.

https://doi.org/10.5194/egusphere-2025-32
Preprint. Discussion started: 21 March 2025

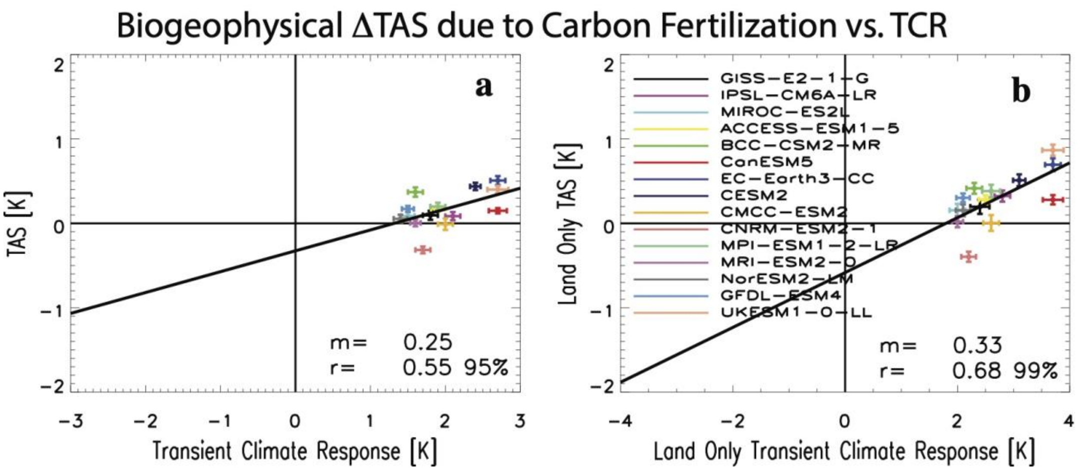

Figure 5. Scatterplots of the global mean near-surface temperature response versus the transient climate response across models. Scatterplots between the (a) global mean near-surface air temperature response (TAS, Y-axis) and the transient climate response (TCR). Panel b is analogous but for land only. Each symbol represents an individual model (see legend). Error bars for each symbol represent the 90% confidence intervals based on a two-tailed pooled t-test. Black line represents the least squares linear regression line. The corresponding slope (m) of the regression and the correlation coefficient (r) are included. Significant correlations based on a two-tailed test at the 95% and 99% confidence level are indicated. Units are K.